An Improved Nonlocal Sparse Unmixing Algorithm for Hyperspectral Imagery

Ruyi Feng, Yanfei Zhong, *Member, IEEE*, and Liangpei Zhang, *Senior Member, IEEE*

***Abstract*—As a result of the spatial consideration of the imagery, spatial sparse unmixing (SU) can improve the unmixing accuracy for hyperspectral imagery, based on the application of a spectral library and sparse representation. To better utilize the spatial information, spatial SU methods such as SU via variable splitting augmented Lagrangian and total variation (SUnSAL-TV) and nonlocal SU (NLSU) have been proposed. However, the spatial information considered in these algorithms comes from the estimated abundance maps, which will change along with the iterations. As the spatial correlations of the imagery are fixed and certain, the spatial relationships obtained from the variable abundances are not reliable during the process of optimization. To obtain more precise and fixed spatial relationships, an improved weight calculation NLSU (I-NLSU) algorithm is proposed in this letter by changing the spatial information acquisition source from the variable estimated abundances to the original hyperspectral imagery. A noise-adjusted principal component analysis strategy is also applied for the feature extraction in the proposed algorithm, and the obtained principal components are the foundation of the spatial relationships. The experimental results of both simulated and real hyperspectral data sets indicate that the proposed I-NLSU algorithm outperforms the previous spatial SU methods.**

***Index Terms*—Hyperspectral imagery, nonlocal, sparse unmixing (SU), spatial information, weight calculation.**

I. Introduction

HYPERSPECTRAL unmixing (HU) is one of the most prominent research areas in hyperspectral data exploitation, as it can infer the components of mixed spectra, known as endmembers, and estimate the proportions (abundances) of the corresponding endmembers [1]–[4]. In conventional spectral unmixing, the endmembers contributing to the mixed pixel are usually assumed to be known in advance, and unmixing can be carried out by solving a constrained linear least squares problem [5]. Unfortunately, what makes the traditional HU fundamentally challenging is the fact that we often do not have any prior knowledge about the endmembers.

Manuscript received April 9, 2014; revised July 22, 2014 and September 25, 2014; accepted October 16, 2014. This work was supported in part by the National Natural Science Foundation of China under Grant 41371344, by the Foundation for the Author of National Excellent Doctoral Dissertation of China (FANEDD) under Grant 201052, and by the Fundamental Research Funds for the Central Universities under Grant 2042014kf00231. *(Corresponding author: Yanfei Zhong).*

The authors are with the State Key Laboratory of Information Engineering in Surveying, Mapping and Remote Sensing, Wuhan University, Wuhan 430079, China (e-mail: zhongyanfei@whu.edu.cn).

Color versions of one or more of the figures in this paper are available online at http://ieeexplore.ieee.org.

Digital Object Identifier 10.1109/LGRS.2014.2367028

Sparse unmixing (SU) is described as a dictionary-based semiblind HU technique, as a result of its application of a spectral library and sparse regression, and it has been widely studied [5]–[11]. Unlike the obligatory requirement for endmembers in the traditional spectral unmixing methods, SU adopts a standard spectral library as its prior knowledge about the endmembers and assumes that the observed hyperspectral remote sensing imagery can be expressed in the form of a linear sparse regression. Due to the potentially large spectral library and the sparse existence of the endmembers in reality, the fractional abundances are often quite sparse. To solve the SU problem, SU via variable splitting augmented Lagrangian (SUnSAL) [6] was proposed and has been successfully applied in spectral unmixing.

As the research into SU has progressed, a number of other spatial SU algorithms have been proposed, such as SU via variable splitting augmented Lagrangian and total variation (SUnSAL-TV) [7] and nonlocal SU (NLSU) [10]. SUnSAL-TV utilizes the spatial information in a first-order pixel neighborhood system, whereas NLSU exploits the spatial contextual information among all the possible self-predictions in the abundance maps. Both sources of spatial information rely on the estimated abundances. Unfortunately, estimated abundances are often inaccurate and variable, as a result of the effect of noise, which leads to inaccurate spatial relationships.

In this letter, to obtain a more accurate and faithful spatial correlation, an improved NLSU (I-NLSU) algorithm is proposed. Since the weight in NLSU acts as the linkage of the spatial information between each nonlocal neighbor, I-NLSU computes the weights from the original imagery and treats the original hyperspectral imagery as a unique and reliable spatial contextual source. For the convenience of nonlocal spatial information extraction or weight calculation, the noise-adjusted principal component analysis (NAPCA) [12] is adopted here for the main spatial correlation extraction. As the original hyperspectral image is fixed, the noise-adjusted principal components are also fixed and can be obtained after the NAPCA process. The spatial relationship or weight can be also determined at the same time. Compared with NLSU computing the optimal abundances with the changing spatial information, I-NLSU improves the computational efficiency and accuracy.

The remainder of this letter is organized as follows. In Section II, NLSU is reviewed, particularly the nonlocal spatial consideration. The I-NLSU algorithm is described in detail in Section III. Section IV presents the experimental results and analysis with three hyperspectral data sets, together with an efficiency analysis of the proposed approach. Finally, the conclusions are drawn in Section V.

II. NLSU

A. SU

$\mathbf{y} \in \mathbf{R}^{L\times 1}$ denotes a mixed pixel, where L is the number of spectral bands; $\mathbf{M} \in \mathbf{R}^{L\times q}$ is the endmember set containing q spectral signatures; and $\boldsymbol{\alpha} \in \mathbf{R}^{q\times 1}$ is the corresponding abundance vector. The linear mixture model (LMM) is shown in the following equation as:

$$\mathbf{y} = \mathbf{M}\boldsymbol{\alpha} + \mathbf{n}. \tag{1}$$

With consideration of the ground truth, the abundance nonnegative constraint (ANC) and the abundance sum-to-one constraint (ASC) [13] are always imposed on the LMM as follows:

$$\alpha_i \geq 0\,(i = 1, 2, \ldots, q) \tag{2}$$

$$\sum_{i=1}^{q} \alpha_i = 1. \tag{3}$$

Differing from obtaining $\mathbf{M}$ by endmember extraction, SU reformulates (1) by using a standard spectral library $\mathbf{A}$ known in advance. Since only a few endmembers of $\mathbf{A}$ will be present in mixed pixels, $\boldsymbol{\alpha}$ contains only a few nonzero values, which means it is sparse [14]. The SU model is rewritten as

$$\mathbf{y} = \mathbf{A}\mathbf{x} + \mathbf{n} \tag{4}$$

where $\mathbf{A} \in \mathbf{R}^{L\times m}$, and $\mathbf{x} \in \mathbf{R}^{m\times 1}$ represents the abundance vector corresponding to the library $\mathbf{A}$. Considering the ANC and ASC, the fully constrained SU optimization problem is defined as:

$$\min_{\mathbf{x}} \|\mathbf{x}\|_0 \text{ s.t. } \|\mathbf{y} - \mathbf{A}\mathbf{x}\|_2 \leq \delta,\ \mathbf{x} \geq 0,\ \mathbf{1}^T\mathbf{x} = 1 \tag{5}$$

where $\|\mathbf{x}\|_0$ is used to calculate the number of nonzero components in vector $\mathbf{x}$, and $\delta \geq 0$ represents the noise or model error. However, since the l_0 term in (5) is a typical NP-hard problem, it can be relaxed to an l_1-norm to obtain the sparsest solution under certain conditions [15]. Therefore, (5) can be equivalent to (6), shown as

$$\min_{\mathbf{x}} \|\mathbf{x}\|_1 \text{ s.t. } \|\mathbf{y} - \mathbf{A}\mathbf{x}\|_2 \leq \delta,\ \mathbf{x} \geq 0,\ \mathbf{1}^T\mathbf{x} = 1 \tag{6}$$

where $\|\mathbf{x}\|_1 = \sum_{i=1}^{m} |x_i|$, and x_i represents the ith abundance in $\mathbf{x}$. To solve (6), SUnSAL and CSUnSAL (the constrained version) were proposed and achieved better results. Unfortunately, both SUnSAL and CSUnSAL focus on analyzing the spectral information without considering any spatial correlations potentially existing in the hyperspectral imagery [7].

B. NLSU

NLSU was proposed based on the basic SU model, and it exploits all possible spatial information in the abundance maps by means of a nonlocal means method [16]. NLSU combines a nonlocal total variation regularizer with the sparse model and makes systematic use of all possible self-predictions of the abundances [10] during the process of abundance optimization.

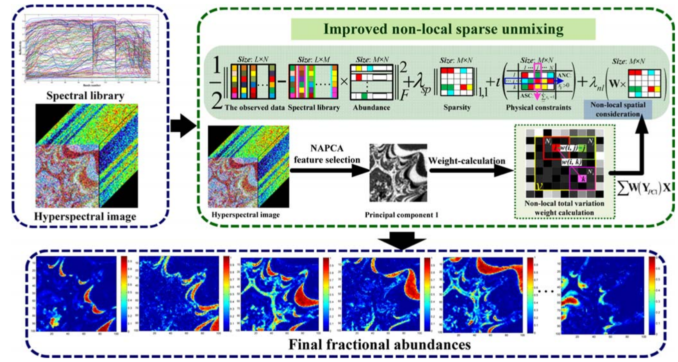

Fig. 1. Flowchart of the I-NLSU algorithm.

The model of the NLSU algorithm is defined as follows:

$$\min_{\mathbf{X}} \frac{1}{2}\|\mathbf{A}\mathbf{X} - \mathbf{Y}\|_F^2 + \lambda_{sp}\|\mathbf{X}\|_{1,1} + \lambda_{nl} J_{\text{NL-TV}}(\mathbf{X}) + \iota_{R_+^m}(\mathbf{X}) + \iota_{\{\mathbf{1}\}}(\mathbf{X}). \tag{7}$$

The definition of the nonlocal spatial term is

$$J_{\text{NL-TV}}(\mathbf{X}_{i,l}) = \sum_j \mathbf{W}_{i,j}(\mathbf{X}_l)\mathbf{X}_{j,l} \tag{8}$$

where $\mathbf{X}_{i,l}$ and $\mathbf{X}_{j,l}$ represent the ith and jth pixel of the lth abundance map. $\mathbf{W}(\mathbf{X}_l)$ denotes the weight of the nonlocal spatial connection between different similar windows of $\mathbf{X}_l$. However, due to the inaccuracies of the estimated abundances during the process of NLSU optimization, the weights change along with the estimated abundances, which will inevitably lead to unreliable spatial correlations and is not compatible with the actual situation. Hence, NLSU can be improved by changing the method of weight calculation.

III. I-NLSU

To exploit the spatial information with a high degree of accuracy in SU, and to make full use of the nonlocal spatial information, an I-NLSU algorithm is proposed. The proposed I-NLSU consists of two steps.

1) The main information (principal components) is obtained by the use of NAPCA from the original hyperspectral imagery, and reliable weights are calculated between different similar windows in the first principal component.
2) The improved NLSU formula based on the improved weights is then optimized.

The schematic of the I-NLSU is illustrated in Fig. 1.

A. The Role of Weight in Non-Local Spatial SU Framework

In non-local spatial SU framework, the nonlocal means total variation regularization term is incorporated into the classical SU model. In the non-local means method, the spatial relationships between each similar window are measured by the degree of similarity, denoted by weight shown as (9)

$$\mathbf{W}_{ij} = \exp\left(-\frac{1}{h^2}\|\mathbf{P}_i - \mathbf{P}_j\|^2\right) \tag{9}$$

where $\mathbf{W}_{ij}$ denotes the weight associated with pixels i and j, and $\mathbf{P}_i$ and $\mathbf{P}_j$ represent the similar windows centered at pixel i and j. $\|\|^2$ acts as the square of the Euclidean distance, and h is a smoothing parameter, controlling the degree of filtering.

As the values of the weight illustrate the connections between the different patches, the critical problem for spatial consideration in the nonlocal spatial SU framework is how to compute the correlations between the nonlocal similar windows to provide accurate and reliable spatial prior knowledge, which is equivalent to finding the exact weights.

B. Comparison of Weight Calculation Methods

Unlike the weight calculation method in the previous NLSU, [shown as (10)], I-NLSU obtains the weights from the original hyperspectral imagery [calculated by (11)]. The method of obtaining weights in I-NLSU is described in detail as follows.

In NLSU, the weight for the final abundances is obtained from the intermediate estimated abundances $(\mathbf{X})$, which are changing all the time. However, the spatial information should be constant in reality. In addition, in the nonlocal means method, the processing objects are always single-band images as one piece of the fractional abundance map serves as the source of the nonlocal spatial correlations. Therefore, in this letter, to get precise information from the original hyperspectral data and to obtain a single-band image, NAPCA [12] is adopted for finding the principal components, in accordance with the image quality. The different weight calculation methods are listed as (10) and (11). Formula (11) is the improved method obtained from the first principal component (PC1), as proposed in this letter

$$\mathbf{W}_{ij} = \exp\left(-\frac{1}{h^2}\|\mathbf{P}(\mathbf{X})_i - \mathbf{P}(\mathbf{X})_j\|^2\right) \quad (10)$$

$$\mathbf{W}_{ij}(\mathbf{Y}_{\mathrm{PC1}}) = \exp\left(-\frac{1}{h^2}\|\mathbf{P}(\mathbf{Y}_{\mathrm{PC1}})_i - \mathbf{P}(\mathbf{Y}_{\mathrm{PC1}})_j\|^2\right) \quad (11)$$

where $\mathbf{P}(\mathbf{X})_i$ and $\mathbf{P}(\mathbf{X})_j$ in (10) represent the similar windows centered at pixels i and j in the abundance map $\mathbf{X}$, and $\mathbf{P}(\mathbf{Y}_{\mathrm{PC1}})_i$ and $\mathbf{P}(\mathbf{Y}_{\mathrm{PC1}})_j$ represent the similar patches centered at pixels i and j in the first principal component (PC1) of the original hyperspectral imagery.

C. Proposed Algorithm and Its Optimization

Based on the constant weights obtained in (11), the nonlocal spatial correlation can be represented as

$$J_{\text{NL-TV}}(\mathbf{X}_{i,l}) = \sum_j \mathbf{W}_{i,j}(\mathbf{Y}_{\mathrm{PC1}})\mathbf{X}_{j,l}. \quad (12)$$

The nonlocal spatial information can be improved based on the reliable weights, and the final fractional abundances can be optimized following model (7) with a fixed spatial similarity degree, joining the sparsity of the abundance and the ASC and ANC. In addition, the split augmented Lagrangian method of multipliers [17] and the alternating direction method of multipliers strategy [18] are employed to efficiently optimize the I-NLSU model.

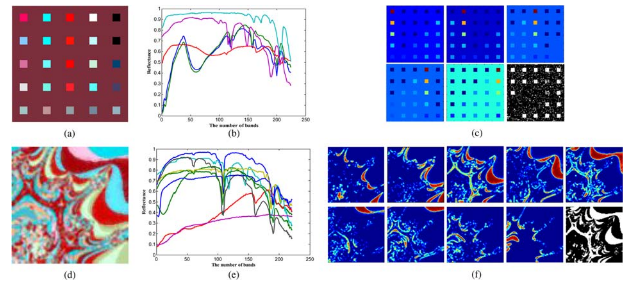

Fig. 2. Simulated data. (a) S-1. (b) Five spectra. (c) Real abundance images and the first PC (grayscale). (d) S-2. (e) Nine spectra. (f) Real abundance images and the first PC (grayscale).

IV. Experiments and Analysis

The I-NLSU algorithm was coded in MATLAB 7.8.0. To evaluate the performance of the proposed method, three hyperspectral data sets were used to make quantitative evaluations. Consistent comparisons were made among SUnSAL, SUnSAL-TV, and NLSU. The accuracy assessment of all the experiments was made by the signal-to-reconstruction error (SRE), defined as

$$\mathrm{SRE} = \frac{E\left[\|\mathbf{x}\|_2^2\right]}{E\left[\|\mathbf{x} - \hat{\mathbf{x}}\|_2^2\right]} \quad (13)$$

$$\mathrm{SRE}\,(\mathrm{dB}) = 10\log_{10}(\mathrm{SRE}). \quad (14)$$

A. Data Preparation

The first two data sets were simulated according to the LMM, and they were both designed based on the U.S. Geological Survey (USGS) spectral library. Simulated data 1 (S-1) was generated following the methodology in [7], with 75×75 pixels and 224 bands per pixel, and five spectral signatures were randomly selected from library $\mathbf{A}$, which is denoted as splib06 (http://speclab.cr.usgs.gov/spectral.lib06). The ASC and ANC were imposed in each simulated pixel. The blocks of the data set were constructed with pure spectral signatures, as well as mixtures ranging between two and five endmembers, and the background pixels were all mixtures of the five endmembers with fixed abundances. Finally, the data were contaminated by Gaussian noise ($\mathrm{SNR} = 10$ dB). The simulated data 2 (S-2), with 100×100 pixels and 221 bands per pixel, was created as a standardized simulated data set for benchmarking the accuracy of the spectral unmixing techniques provided in the HyperMix tool [19]. The nine endmembers for the simulation were randomly selected from the USGS library after removing certain bands. Finally, zero-mean Gaussian noise was added ($\mathrm{SNR} = 10$ dB). Fig. 2 shows the two simulated datasets.

The real hyperspectral data set (R-1) is a 128×64 subset, with 46 bands in each pixel, which was acquired by the Nuance NIR imaging spectrometer (650–1100 nm and 10-nm spectral interval) in November 2013. The spectral library used for R-1 was collected from other Nuance data sets obtained by the same spectrometer during the same time period and contains 70 pure materials. R-1 consists of more than eight kinds of land cover, including wood (1), fresh grass (2), dead leaves (3), gravel (4), background (5), shadow (6), ceramic bowl (7), and acrylic shoelaces (8), as shown in Fig. 3(d). To better

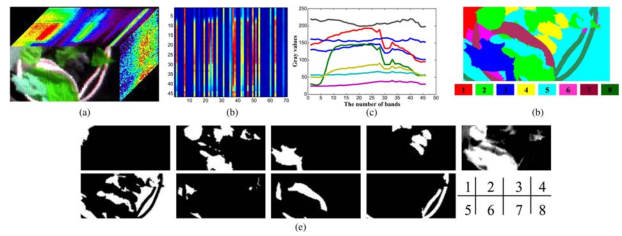

Fig. 3. R-1 data set. (a) R-1. (b) Spectral library. (c) Eight spectra. (d) Classification result. (e) Approximate true abundance maps and the first PC obtained from NAPCA (upper right).

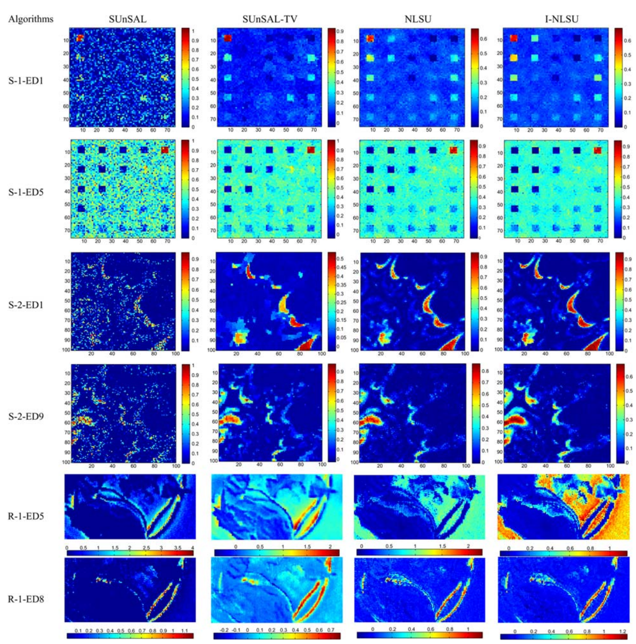

Fig. 4. Estimated abundances of the endmembers for S-1, S-2, and R-1.

assess the performance of the unmixing algorithms, a high-spatial-resolution digital image of the same scene was taken on the same day with a digital camera (384×192) , and this image was used for reference of the ground truth [20]. After geometrical calibration, objected-oriented classification, and downsampling were undertaken, the approximate true abundance maps were obtained.

B. Results and Analysis

The performance of the proposed I-NLSU was tested using the above three hyperspectral data sets. Parts of the results obtained from S-1, S-2, and R-1 with the SUnSAL, SUnSAL-TV, NLSU, and I-NLSU algorithms are shown in Fig. 4 and the quantitative assessments are listed in Table I.

In Fig. 4, the estimated abundance maps show the effectiveness of each algorithm. For the abundance maps of the S-1-ED1 endmember, the abundance values of the background are all 0.1149, whereas the values in the second column (first line) of squares are all 0 (the same as the third column, first line, and the fourth and the fifth columns, first line) and are therefore smaller than the background's abundances and should be darker than the background. However, due to the impact of the total variation regularization or nonlocal means (including nonlocal total variation) spatial consideration methods, the squares near the first column and the first line of squares (whose abundance

TABLE I
SRE (IN DECIBELS) VALUES OF THE ESTIMATED ABUNDANCE MAPS

Dataset	SUnSAL	SUnSAL-TV	NLSU	I-NLSU
S-1	3.9402	13.6437	13.8338	**14.6913**
S-2	4.5724	8.2779	9.9863	**10.2450**
R-1	1.4692	2.2645	3.0508	**3.3991**

values are all 1), together with their neighborhood pixels, are all smoothed, and the abundance values are changed to be bigger than the truth, which is the same as with S-1-ED5 and S-2-ED9.

In general, it is shown in Fig. 4 that I-NLSU can obtain more accurate abundances than the other two spatial SU methods, SUnSAL-TV and NLSU, as their spatial correlations are acquired from the variable estimated abundances, which change in the optimization process. However, the I-NLSU algorithm can precisely capture most of the spatial relationships from the original hyperspectral imagery after the feature selection strategy, NAPCA, and fortunately, the correlations are definite and more exact, which can be proved from the results in Fig. 4. In summary, the improvements are due to the special method of weight calculation.

Taking S-2-ED9 in Fig. 4 as an example, it can be seen that the abundances obtained from I-NLSU are closer to the true abundances, particularly in the details, background, and homogeneous regions. Furthermore, for S-2-ED1 with SUnSAL-TV, the final abundance map seems to be much smoother to obtain the highest SRE (in decibels), and the highest abundance is only 0.5395, which is much less than the original highest abundance truth of 1. However, NLSU and I-NLSU achieve relatively accurate results, which are closer to 1.

In addition, the ASC and ANC are often imposed on the objective function in unmixing problems due to the physical composition of a mixed pixel. The two constraints work well for simulated data sets as they are simulated under restrictive assumptions; however, the reality is often different. This is why the abundance values may have some negative values or values greater than 1, and the maps display negative and/or abundance values greater than 1, such as R-1-ED8, in the real hyperspectral data set.

Compared with the classical SU method, i.e., SUnSAL, the spatial SU approaches, i.e., SUnSAL-TV, NLSU, and I-NLSU, show prominent superiority in noise suppression, particularly in the background and large homogenous areas, because they not only consider the sparsity of the abundance maps but also exploit the spatial prior information. Due to the poor quality of the original image, the weights obtained from the principal components are inevitably influenced. However, the final abundances of I-NLSU have suppressed many outliers and obtained a much smoother characterization than the other approaches. The unmixing results of R-1 illustrate the different characteristics of each algorithm. Compared with the spatial SU techniques, SUnSAL only focuses on the spectral analysis and neglects the important neighborhood relationships, leading to insufficient consideration of each endmember, and lower SRE (in decibels) values.

Table I lists the SRE (in decibels) values of the above hyperspectral data sets and gives a quantitative assessment for the performance of SUnSAL, SUnSAL-TV, NLSU, and I-NLSU. The SRE (in decibels) values of I-NLSU are clearly higher than those of the other methods, improving the SRE

TABLE II
EXECUTION TIMES OF NLSU AND I-NLSU FOR S-1, S-2, AND R-1

Time [s]	S-1	S-2	R-1
NLSU	46.4883	73.7885	112.1959
I-NLSU	45.1467	70.6217	75.8789

(in decibels) from 3.9402, 4.5724, and 1.4692 of SUnSAL to 14.6913, 10.2450, and 3.3991 for S-1, S-2, and R-1, respectively. The table also indicates the importance of spatial consideration in the unmixing problem, in which all the spatial SU methods exhibit advantages over the classical SU technique, SUnSAL. With regard to the NLSU algorithm, the SRE (in decibels) values obtained from I-NLSU are a little higher, and the improvements are mainly due to the novel method of weight calculation in the nonlocal means spatial consideration. Generally speaking, the proposed I-NLSU can better suppress outliers in the spatial consideration and can efficiently increase the unmixing accuracy.

C. Efficiency Analysis

Due to the different methods of obtaining the spatial correlations, the execution times of NLSU and I-NLSU are different. In I-NLSU, the definite nonlocal relationships, or the weights, can be obtained as soon as the NAPCA process is completed, and we then save them in memory. Hence, during the following optimization calculation, the weights can be reused in the process of iteration. However, the NLSU algorithm needs to compute the weights following the updating of the estimated abundances. Since the difference between NLSU and I-NLSU lies in the method of weight computation, the efficiency of I-NLSU is much higher than that of NLSU.

To illustrate the efficiency, Table II lists the execution times of NLSU and I-NLSU for S-1, S-2, and R-1. All the algorithms were implemented using MATLAB 7.8.0 on a desktop PC equipped with an Intel Core i3-2100 CPU (at 3.10 GHz) and 8.00 GB of RAM. It can be observed in Table II that the execution times of I-NLSU are all less than for NLSU. A significant decrease in execution time appears in the R-1 data set, which was set as 200 times iterations in the experiment, whereas the other simulated data sets were all set as 100 times. The main reason for the small gap in execution time between NLSU and I-NLSU lies in the Visual C++ 6.0 programming platform, on which the weight computing process is coded as the efficiency is quite high.

V. CONCLUSION

In this letter, an improved NLSU algorithm (I-NLSU) has been proposed. Unlike the previous spatial SU approaches, which obtain the spatial correlations from the estimated abundances, I-NLSU exploits the fixed spatial information from the original imagery by the use of the NAPCA feature selection strategy. To illustrate the advantage of I-NLSU, SUnSAL, SUnSAL-TV, and NLSU were used as a comparison with both simulated and real hyperspectral datasets. Due to the accurate weights derived from the original imagery, I-NLSU achieved better unmixing results with both the simulated and the real data sets. The experimental results also confirm the ability of I-NLSU to consider the spatial relationships in spectral unmixing. In addition, the novel weight calculation method for the non-local spatial consideration improves the efficiency of the NLSU approach. Our future research will address the computational complexity, and more real hyperspectral data sets will be utilized to further test the I-NLSU algorithm.

ACKNOWLEDGMENT

The authors thank the research group supervised by Prof. J. M. Bioucas-Dias and Prof. A. Plaza for sharing their algorithms for comparison purposes together with the AVIRIS data. They also thank the reviewers for their helpful comments.

REFERENCES

[1] J. M. Bioucas-Dias *et al.*, “Hyperspectral remote sensing data analysis and future challenges,” *IEEE Geosci. Remote Sens. Mag.*, vol. 1, no. 2, pp. 6–36, Jun. 2013.
[2] Q. Tong, Y. Xue, and L. Zhang, “Progress in hyperspectral remote sensing science and technology in China over the past three decades,” *IEEE J. Sel. Topics Appl. Earth Observ. Remote Sens.*, vol. 7, no. 1, pp. 70–91, Jan. 2014.
[3] J. M. Bioucas-Dias *et al.*, “Hyperspectral unmixing overview: Geometrical, statistical, and sparse regression-based approaches,” *IEEE J. Sel. Topics Appl. Earth Observ. Remote Sens.*, vol. 5, no. 2, pp. 354–379, Apr. 2012.
[4] A. Plaza, Q. Du, J. Bioucas-Dias, X. Jia, and F. Kruse, “Foreword to the special issue on spectral unmixing of remotely sensed data,” *IEEE Trans. Geosci. Remote Sens.*, vol. 49, no. 11, pp. 4103–4110, Nov. 2011.
[5] W. K. Ma *et al.*, “A signal processing perspective on hyperspectral unmixing: Insights from remote sensing,” *IEEE Signal Process. Mag.*, vol. 31, no. 1, pp. 67–81, Jan. 2014.
[6] M. D. Iordache, J. M. Bioucas-Dias, and A. Plaza, “Sparse unmixing of hyperspectral data,” *IEEE Trans. Geosci. Remote Sens.*, vol. 49, no. 6, pp. 2014–2039, Jun. 2011.
[7] M. D. Iordache, J. M. Bioucas-Dias, and A. Plaza, “Total variation spatial regularization for sparse hyperspectral unmixing,” *IEEE Trans. Geosci. Remote Sens.*, vol. 50, no. 11, pp. 4484–4502, Nov. 2012.
[8] X. Zhao, F. Wang, T. Huang, M. K. Ng, and R. J. Plemmons, “Deblurring and sparse unmixing for hyperspectral images,” *IEEE Trans. Geosci. Remote Sens.*, vol. 51, no. 7, pp. 4045–4058, Jul. 2013.
[9] M. D. Iordache, J. Bioucas-Dias, and A. Plaza, “Collaborative sparse regression for hyperspectral unmixing,” *IEEE Trans. Geosci. Remote Sens.*, vol. 52, no. 1, pp. 341–354, Jan. 2014.
[10] Y. Zhong, R. Feng, and L. Zhang, “Non-local sparse unmixing for hyperspectral remote sensing imagery,” *IEEE J. Sel. Topics Appl. Earth Observ. Remote Sens.*, vol. 7, no. 6, pp. 1889–1909, Jun. 2014.
[11] M. D. Iordache, J. Bioucas-Dias, A. Plaza, and B. Somers, “MUSIC-CSR: Hyperspectral unmixing via multiple signal classification and collaborative sparse regression,” *IEEE Trans. Geosci. Remote Sens.*, vol. 52, no. 7, pp. 4364–4382, Jul. 2014.
[12] C.-I. Chang and Q. Du, “Interference and noise-adjusted principal components analysis,” *IEEE Trans. Geosci. Remote Sens.*, vol. 37, no. 5, pp. 2387–2396, Sep. 1999.
[13] D. C. Heinz and C.-I. Chang, “Fully constrained least squares linear spectral mixture analysis method for material quantification in hyperspectral imagery,” *IEEE Trans. Geosci. Remote Sens.*, vol. 39, no. 3, pp. 529–545, Mar. 2001.
[14] M. D. Iordache, “A sparse regression approach to hyperspectral unmixing,” Ph.D. dissertation, School Elect. Comput. Eng., Instituto Superior Técnico, Lisbon, Portugal, 2011.
[15] E. Candès and J. J. Romberg, “Sparsity and incoherence in compressive sampling,” *IEEE Trans. Image Process.*, vol. 23, pp. 969–985, Apr. 2007.
[16] A. Buades, B. Coll, and J. M. Morel, “A non-local algorithm for image denoising,” in *Proc. IEEE CVPR*, 2005, vol. 2, pp. 60–65.
[17] J. Eckstein and D. Bertsekas, “On the Douglas–Rachford splitting method and the proximal point algorithm for maximal monotone operators,” *Math. Progr.*, vol. 55, no. 1–3, pp. 293–318, Apr. 1992.
[18] J. Bioucas-Dias and M. Figueiredo, “Alternating direction algorithms for constrained sparse regression: Application to hyperspectral unmixing,” in *Proc. 2nd WHISPERS*, Reykjavik, Iceland, 2010, pp. 1–4.
[19] L. I. Jimenez, G. Martin, and A. Plaza, “A new tool for evaluating spectral unmixing applications for remotely sensed hyperspectral image analysis,” in *Proc. Int. Conf. GEOBIA*, Rio de Janeiro, Brazil, 2012, pp. 1–5.
[20] X. Xu, Y. Zhong, L. Zhang, and H. Zhang, “Sub-pixel mapping based on a MAP model with multiple shifted hyperspectral imagery,” *IEEE J. Sel. Topics Appl. Earth Observ. Remote Sens.*, vol. 6, no. 2, pp. 580–593, Apr. 2013.